Pulse-width-tunable 0.7 W mode-locked Cr: forsterite laser

A. A. Ivanov,[1,2] A. A. Voronin,[1,3] A. A. Lanin,[1,3] D. A. Sidorov-Biryukov,[1,3] A. B. Fedotov,[1,3] and A. M. Zheltikov[1,2,3,4]

[1]*Physics Department, International Laser Center, M.V. Lomonosov Moscow State University, Moscow 119992, Russia*

[2]*Center of Photochemistry, Russian Academy of Sciences, ul. Novatorov 7a, Moscow 117421, Russia*

[3]*Russian Quantum Center, ul. Novaya 100, Skolkovo, Moscow Region 1430125, Russia*

[4]*Department of Physics and Astronomy, Texas A&M University, College Station Texas 77843-4242, USA*

**Corresponding author: zheltikov@physics.msu.ru*

Received October 7, 2013; revised November 24, 2013; accepted November 25, 2013; posted November 25, 2013 (Doc. ID 198971); published January 3, 2014

A mode-locked chromium forsterite laser with output power in excess of 0.7 W, a central wavelength of 1.25 μm, a pulse repetition rate of 29 MHz, and an output pulse-width-tunable from 40 to 200 fs is demonstrated. The dynamics behind the buildup of ultrashort light pulses in this laser is shown to involve spectral and temporal breathing due to the interplay of gain, Kerr nonlinearity, and dispersion effects. The pulse-width-tunable 1.25 μm output delivered by the developed laser source suggests a powerful tool for nonlinear-optical bio-imaging and offers an advantageous front end for extreme-power laser technologies.

OCIS codes: (190.7110) Ultrafast nonlinear optics; (140.7090) Ultrafast lasers.
http://dx.doi.org/10.1364/OL.39.000205

Mode-locked chromium forsterite laser systems [1–5] are gaining prominence as advantageous sources of ultrashort pulses offering unique options for a broad class of optical technologies. With the spectrum of a short-pulse Cr: forsterite laser output centered at 1.25 μm, such lasers help achieve larger penetration depth in biological tissues [6] and allow third-harmonic generation [7,8] in the spectral region where the attenuation of the third harmonic is not as dramatic as it is for Ti: sapphire laser pulses. Mode-locked Cr: forsterite lasers integrated with photonic-crystal fiber wavelength shifters and supercontinuum sources have been shown to provide a powerful tool for time-resolved studies of ultrafast processes in molecular aggregates and carbon nanotubes [9], as well as for the coherent excitation and probing of optical phonon modes in solid-state photonics [10].

Chromium forsterite lasers also promise to fill their niche in ultrafast optical technologies. With specially designed chirped mirrors, a Cr: forsterite laser oscillator can deliver light pulses as short as 14 fs [5], which correspond to approximately three field cycles at 1.3 μm. An average power as high as 1.4 W has been achieved for a sub-100 fs output of a Cr: forsterite laser oscillator [11], and peak powers as high as 425 kW have been demonstrated [12].

Here we demonstrate a mode-locked Cr: forsterite laser that combines 40-to-200 fs pulse-width tunability with a peak power of 0.6 MW and an output average power in excess of 0.7 W at a pulse repetition rate of 29 MHz. We show that the dynamics behind the buildup of ultrashort light pulses in this laser involves spectral and temporal breathing due to the interplay of gain, Kerr nonlinearity, and dispersion effects. The pulse-width-tunable 1.25 μm output delivered by the developed laser source offers a powerful tool for nonlinear-optical bio-imaging and suggests attractive solutions for extreme-power laser technologies.

Our chromium forsterite laser oscillator employs a z-fold cavity design (Fig. 1), which is intended to increase the cavity length for higher output energy. A 17 mm long $Cr^{4+}:Mg_2SiO_4$ crystal is pumped with an 8 W laser-diode-pumped ytterbium fiber laser output at 1030 nm. The laser crystal, cooled down to 278 K, is located between a pair of 100 mm curvature-radius focusing mirrors. In agreement with the earlier studies [11,13], an increase in the temperature of the forsterite crystal in our system reduced the lifetime of the upper laser state and decreased the quantum yield of fluorescence. A semiconductor saturable-absorber mirror (SESAM) with a response time of 2 ps and modulation depth of 0.025 is used as a rear reflector of the laser cavity. Radiation is coupled out of the cavity through a 10% mirror. The net cavity dispersion is adjusted with a pair of SF57 prisms, separated by distance d and placed either in front of the SESAM rear mirror (scheme 1) or in front of the output coupler (scheme 2).

Short-pulse operation of the laser cavity was analyzed in the framework of the 1D pulse-evolution model [14,15], which includes dispersion, saturable gain, Kerr nonlinearity, self-steepening, and saturable absorption inside the laser cavity. The buildup of the laser pulse in the laser crystal is described by the equation

$$\frac{\partial}{\partial z}A(\omega,z) = i\hat{D}(\omega)A(\omega,z) + \hat{F}\left[i\gamma_0\hat{T}|A(\eta,z)|^2A(\eta,z) - \frac{q_0}{1+P(\eta,z)/P_{\mathrm{sat}}}A(\eta,z)\right] + \frac{g(\omega)\,A\,(\eta,z)}{1+W(z)/W_{\mathrm{sat}}}, \quad (1)$$

where $A(\eta,z)$ is the field amplitude, $A(\omega,z)$ is its Fourier transform, η is the time in the retarded frame of reference, ω is the frequency, z is the coordinate along the cavity, $P(z) = |A(\eta,z)|^2$ is the power, $W(z) = \int_{-T_R/2}^{T_R/2}|A(\eta,z)|^2 d\eta$ is the energy, T_R is the cavity round-trip time, $\hat{D}(\omega) = k_2(\omega-\omega_0)^2/2 + k_3(\omega-\omega_0)^3/6$ is the dispersion operator, ω_0 is the central frequency, $k_2 = \partial^2k/\partial\omega^2|_{\omega_0}, k_3 = \partial^3k/\partial\omega^3|_{\omega_0}$, are the second- and

third-order dispersion coefficients, $k(\omega)$ is the wave number, γ_0 is the nonlinear coefficient at the frequency ω_0, c is the speed of light, γ_0 is the nonlinear coefficient, $T = 1 + i\omega_0^{-1}\partial/\partial\eta$, $g(\omega) = g_0[1 - (\omega - \omega_0)^2/\Delta\omega^2]$ is the gain, g_0 is the small-signal gain, $\Delta\omega$ is the gain bandwidth, W_{sat} is the gain saturation energy, q_0 is the mode-locking parameter, and P_{sat} is the mode-locking saturation power. Dispersion of the laser crystal is included in the model through the data from [16]. The dispersion of the prism pair was included [15] by adding a spectral phase $A'(\omega,z) = A(\omega,z)\exp\{i[\beta_2(\omega-\omega_0)^2 + \beta_3(\omega-\omega_0)^3]\}$, where β_2 and β_3 are the coefficients [17] in the terms accounting for the quadratic and cubic phase induced by a round trip through the prism pair. The saturable absorber was included in simulations through the model developed in [18].

The interplay of the gain with nonlinear optical and dispersion effects translates into characteristic breathing dynamics of the key parameters of the laser pulse building up inside the laser cavity. This dynamic is clearly seen in Figs. 2 and 3, showing how the pulse width, the bandwidth, and the pulse energy change along the laser cavity. When passing through the laser crystal from point A to point B (shown in Fig. 1), the laser pulse experiences amplification and self-phase modulation (SPM) due to the Kerr nonlinearity of the laser crystal, giving rise to the increase in the energy [Fig. 2(b)], field intensity [Figs. 3(a) and 3(b)], and the bandwidth [Figs. 2(a), 3(e), and 3(f)] of the laser pulse. The positive chirp induced by SPM is then compensated by the prism pair [cf. Figs. 3(f) and 3(g)], giving rise to the shortest pulse width inside the cavity [Figs. 2(a) and 3(c)], which is observed at point C (Fig. 1). When the net dispersion of the cavity is set at $\beta_{\text{net}} \approx -1560$ fs^2, the pulse width

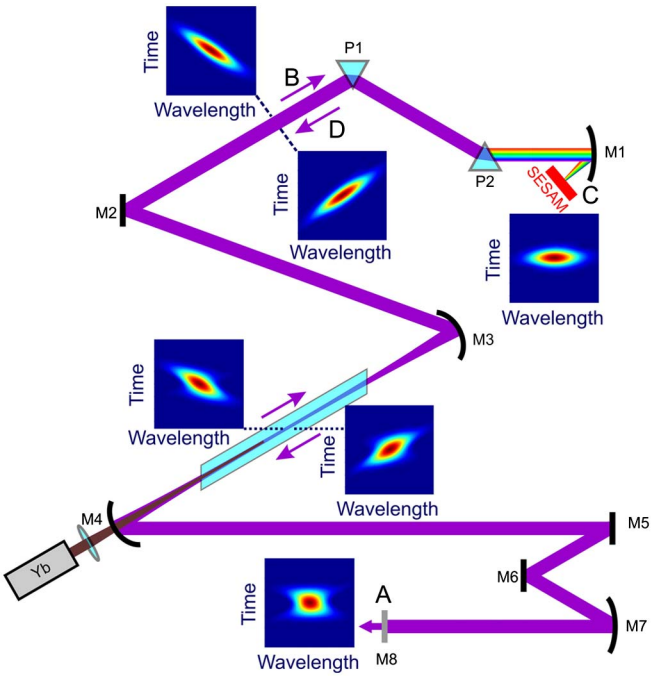

Fig. 1. Diagram of the Cr: forsterite laser with spectrograms calculated for reference points inside the laser cavity: Cr: F, Cr: forsterite crystal; P1 to P2, prisms; M1 to M8, mirrors; Yb, ytterbium fiber pump laser.

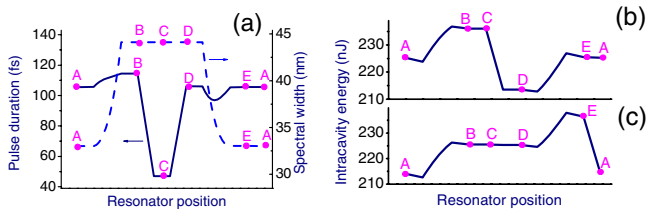

Fig. 2. Pulse width (solid line) and the bandwidth (dashed line) of the laser pulse (a) and the pulse energy (b) and (c) at different points inside the Cr: forsterite laser cavity in scheme 2 (b) and scheme 1 (c) with $\gamma_0 = 0.45$ MW^{-1} cm^{-1}, $k_2 = 490$ fs^2/cm, $k_3 = 1680$ fs^3/cm, $\beta_2 = -3220$ fs^2, $\beta_3 = -6270$ fs^3, $d = 39$ cm, $q = 0.4$ mm^{-1}, $P_{\text{sat}} = 2.5$ MW, $g_0 = 4$ cm^{-1}, $W_{\text{sat}} = 7.8$ nJ, and $\beta_{\text{net}} = -1560$ fs^2. The spectral-bandwidth and spectral-width curves in panel (a) for schemes 1 and 2 are almost indistinguishable.

of a laser pulse at point C is 47 fs [Figs. 2(a) and 4(b)], which is only 3 fs longer than the transform-limited pulse width [cf. the solid and dashed lines in Fig. 4(b)] supported by the entire spectrum of the pulse behind the laser crystal [Fig. 4(d)].

On its way back from point C to point D, the pulse acquires a negative chirp due to the dispersion of the prisms [Figs. 3(d) and 3(h)]. Amplification of such a negatively chirped pulse in the laser crystal is accompanied by spectral narrowing due to the Kerr nonlinearity of the laser crystal [the DA section in Fig. 2(a)], which recovers the pulse we started with at point A. For $\beta_{\text{net}} \approx -1560$ fs^2 (Figs. 2–4), the pulse at this point has a pulse width of 106 fs [the solid line in Fig. 4(a)], while the transform-limited pulse width supported by the entire spectrum of the pulse in this section of the laser cavity [Fig. 4(c)] is 54 fs [the dashed line in Fig. 4(a)]. The output pulse widths and energies measured in experiments for both laser schemes agree well with the results of simulations [Figs. 4(c) and 5(a)]. Within this range of parameters, the SESAM mirror serves to suppress the cw radiation component and increases the threshold for the two-pulse regime, but does not have any noticeable influence on the evolution of the pulse width and spectral width along the laser cavity.

The shortest pulse width and the highest peak power of the laser output are achieved when the nonlinear phase shift acquired by the light pulse inside the laser cavity is precisely balanced by the dispersion-induced phase shift. This argument is illustrated by simulations presented in Fig. 3, showing the temporal shapes and spectra of the laser pulse along with its temporal and spectral phase at the key points inside the laser cavity. The gain, nonlinearity, and dispersion inside the cavity are adjusted in such a way that, at the points A and C, i.e., on the cavity mirrors, the laser pulse has an almost flat phase [Figs. 3(a), 3(c), 3(e), and 3(g), where an ideally flat phase is shown by the dashed–dotted line). The nonlinear phase $\varphi_{\text{SPM}} = \gamma_0|A|^2L$ due to SPM inside the laser crystal with length L [dashed–dotted line in Fig. 3(b)] is accurately compensated, as can be seen from Fig. 3, as well as from the spectrograms in Fig. 1, by the phase induced by intracavity dispersion, which is dominated by the tunable dispersion of the prisms [shown by the dashed–dotted line in Figs. 3(f) and 3(h)] and in-

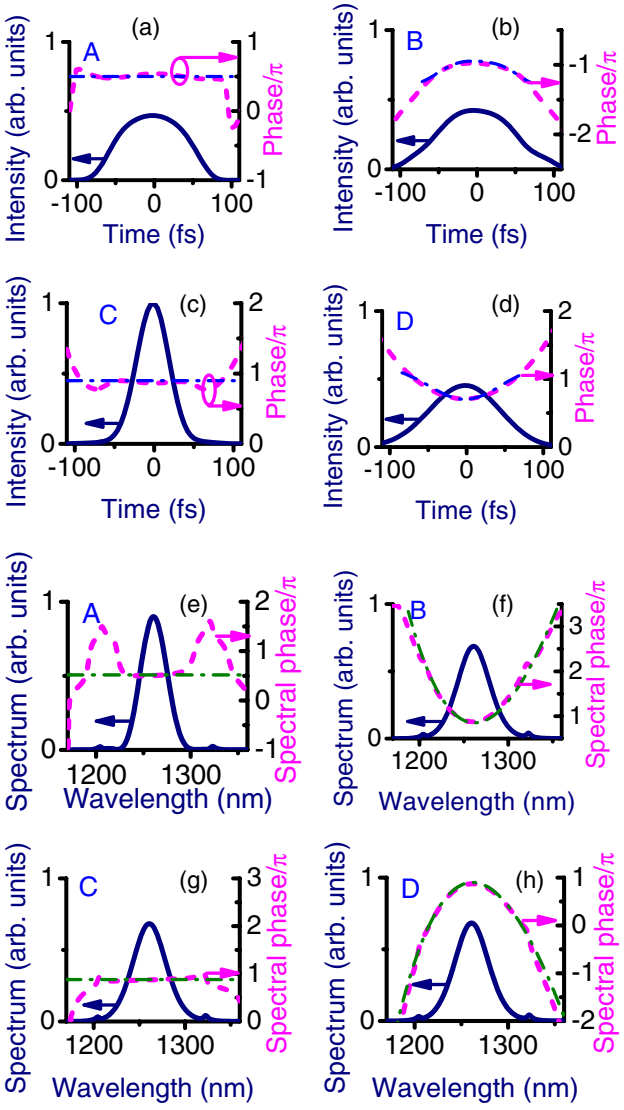

Fig. 3. Evolution of (a)–(d) the pulse envelope (navy solid line) and temporal phase (pink dashed line), as well as (e) through (h) the spectrum (navy solid line) and the spectral phase (pink dashed line) at the points A (a) and (e); B (b) and (f); C (c) and (g); D (d) and (h) in the Cr: forsterite laser cavity with parameters as specified in Fig. 2. Blue and green dashed–dotted lines show an ideally flat phase (a), (c), (e), and (g), the phase φ_{SPM} (b) and $-\varphi_{SPM}$ (d) induced by SPM in the laser crystal, and the phase induced by the dispersion of the prisms (f) and (h).

cludes a constant component due to the dispersion of the laser crystal. With the dispersion of the Cr: forsterite crystal fixed, dispersion compensation by a prism pair is possible only for moderate field intensities.

When the nonlinear phase profile becomes too complicated so that it can no longer be approximated by a low-order polynomial, more sophisticated dispersion compensation components, e.g., specially designed chirped mirrors [5], would be necessary.

Overall, the pulse dynamics in our laser was consistent with the dispersion-management scenario [19], with the TBP of the laser pulses with the shortest pulse width and maximum peak power being close to the TBP of a hyperbolic-secant pulse, indicating an optimal balance

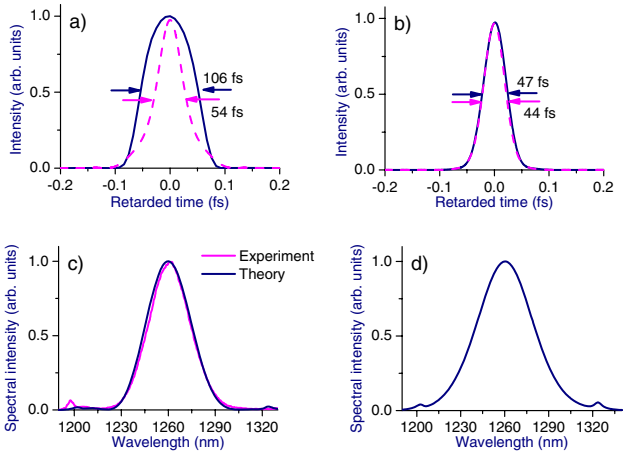

Fig. 4. Pulse width (a) and (b) and spectra (c) and (d) of the laser pulse at points A (a) and (c) and C (b) and (d) in the Cr: forsterite laser cavity with parameters as specified in Fig. 2. Transform-limited pulses are shown by the dashed line. The experimental spectrum (red line) is shown versus simulations (blue line) in panel (c).

between dispersion and nonlinearity. However, a periodic perturbation of the laser pulse by the gain and saturable absorption inside the cavity at this level of peak powers and pulse widths was found to induce a parametric instability, which can lead to a breakup of the laser pulse [20]. In the frequency domain, this

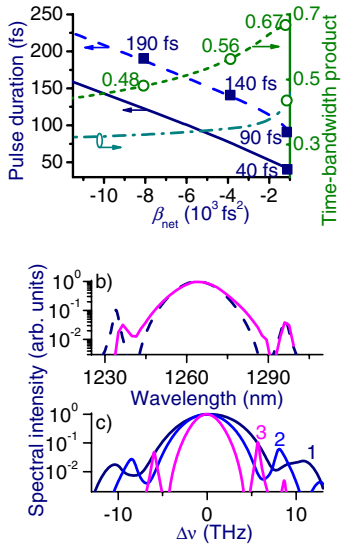

Fig. 5. (a) Output pulse width (solid and dashed lines) and the time–bandwidth product (dotted and dashed–dotted lines) for a Cr: forsterite laser as a function of the net cavity dispersion for scheme 1 (dashed and dotted lines) and scheme 2 (solid and dashed–dotted lines) with laser parameters as specified in Fig. 2: (lines) simulations, (dots) experimental results. (b) Experimental (solid line) and theoretical (dashed line) output spectra for $\beta_2 = -8860$ fs^2, $\beta_3 = -15850$ fs^3, $d = 83$ cm, and $\beta_{net} = -7200$ fs^2 and (c) The laser output spectra for (curve 1) $\beta_2 = -3220$ fs^2, $\beta_3 = -6270$ fs^3, and $\beta_{net} = -1560$ fs^2, $d = 39$ cm, (curve 2) $\beta_2 = -4630$ fs^2, $\beta_3 = -8670$ fs^3, $d = 50$ cm, and $\beta_{net} = -4630$ fs^2, and (curve 3) $\beta_2 = -8860$ fs^2, $\beta_3 = -15850$ fs^3, $d = 83$ cm, and $\beta_{net} = -7200$ fs^2 with $\gamma_0 = 0.54\,\mathrm{MW^{-1}\,cm^{-1}}$, $k_2 = 490\,\mathrm{fs^2/cm}$, $k_3 = 1680\,\mathrm{fs^3/cm}$, $q = 1.0\ \mathrm{mm^{-1}}$, $P_{sat} = 2.5$ MW, $g_0 = 4\ \mathrm{cm^{-1}}$, and $W_{sat} = 17.8$ nJ.

modulation-instability-type effect is manifested in well-resolved spectral sidebands observed on either side of the maximum in the laser spectrum. The frequencies of these sidebands, often referred to as the Kelly sidebands, which are clearly seen in experimental laser spectra [Figs. 4(c) and 5(b)] and accurately reproduced by our simulations [cf. the solid and dashed curves in Fig. 5(b)], are highly sensitive to the net cavity dispersion. Decreasing the cavity dispersion in its absolute value [from -7200 fs^2 to -1560 fs^2 in Fig. 5(c)], we increase the frequency offset of the Kelly sidebands from the central laser frequency from 5.5 to 10.5 THz [cf. curves 1 to 3 in Fig. 5(c)], thus extending the stability range of laser pulses toward shorter pulse widths.

The pulse width on the mirrors of the laser cavity, that is, at points A and C (Fig. 1), can be smoothly tuned by varying the cavity dispersion. In particular, as the absolute value of the net cavity dispersion β_{net} is tuned from -1200 fs^2 to -8800 fs^2, the pulse width increases from 90 to 200 fs at point A and from 40 to 125 fs at point C [Fig. 5(a)], with the time–bandwidth product (TBP) of these pulses varying as shown by the dotted and dashed–dotted lines in Fig. 5(a). With an appropriate adjustment of the pump power, the output laser energy could be kept almost constant at least in the range of net cavity dispersion values from -1500 fs^2 to -9500 fs^2, yielding a maximum energy of about 245 nJ at point C in a laser with a 10% outcoupling mirror. Such a laser delivers output pulses with energy above 24 nJ at a pulse-repetition rate of 29 MHz, corresponding to an average output power above 0.7 W. In scheme 2, where the output pulse width is 40 fs in this regime [solid line in Fig. 5(a)], the output peak power is 0.6 MW, which is substantially higher than the level of peak powers achieved in the earlier work. Typical results of autocorrelation pulse-width measurements performed at this level of Cr: forsterite laser output energies [rectangles in Fig. 5(a)] agree well with the results of simulations [solid and dashed lines in Fig. 5(a)].

In its output peak power, pulse repetition rate, and the attainable range of pulse widths, the Cr: forsterite laser demonstrated in this work is ideally suited for a broad class of nonlinear-optical bio-imaging applications [6,7], including nonlinear-optical brain imaging [8]. Pulse and bandwidth tunability of the short-pulse Cr: forsterite laser output drastically enhance the versatility of such lasers, allowing, e.g., a single compact mode-locked Cr: forsterite oscillator to be used in multiphoton/harmonic-generation and coherent Raman modes of imaging. Such field waveforms can be further broadened and wavelength-shifted using photonic-crystal fibers [21], enabling the creation of practical sources for nonlinear-optical imaging and opening the ways toward the development of compact single-cycle waveform synthesizers. In extreme-power laser technologies, the central wavelength of short-pulse Cr: forsterite laser output hits an ultrabroadband phase-matching region for nonlinear-optical crystals [22], enabling optical parametric chirped-pulse amplification of extremely short-field waveforms.

This research was supported in part by the Russian Foundation for Basic Research (project nos. 13-02-92115, 13-02-01465, and 13-04-40335), the Welch Foundation (grant no. A-1801), and the Skolkovo Foundation (grant no. 78).

References

1. A. Seas, V. Petričević, and R. R. Alfano, Opt. Lett. **18**, 891 (1993).
2. V. Yanovsky, Y. Pang, F. Wise, and B. I. Minkov, Opt. Lett. **18**, 1541 (1993).
3. Z. Zhang, K. Torizuka, T. Itatani, K. Kobayashi, T. Sugaya, T. Nakagawa, and H. Takahashi, Opt. Lett. **23**, 1465 (1998).
4. A. A. Ivanov, M. V. Alfimov, and A. M. Zheltikov, Laser Phys. **10**, 796 (2000).
5. C. Chudoba, J. G. Fujimoto, E. P. Ippen, H. A. Haus, U. Morgner, F. X. Kärtner, V. Scheuer, G. Angelow, and T. Tschudi, Opt. Lett. **26**, 292 (2001).
6. G. J. Tearney, M. E. Brezinski, B. Bouma, S. Boppart, C. Pitris, J. F. Southern, and J. G. Fujimoto, Science **276**, 2037 (1997).
7. S.-W. Chu, S.-Y. Chen, T.-H. Tsai, T.-M. Liu, C.-Y. Lin, H.-J. Tsai, and C.-K. Sun, Opt. Express **11**, 3093 (2003).
8. L. V. Doronina-Amitonova, A. A. Lanin, O. I. Ivashkina, M. A. Zots, A. B. Fedotov, K. V. Anokhin, and A. M. Zheltikov, Appl. Phys. Lett. **99**, 231109 (2011).
9. A. A. Ivanov, M. V. Alfimov, and A. M. Zheltikov, Usp. Fiz. Nauk. **174**, 743 (2004).
10. A. D. Savvin, A. A. Lanin, A. A. Voronin, A. B. Fedotov, and A. M. Zheltikov, Opt. Lett. **35**, 919 (2010).
11. S.-H. Chia, T.-M. Liu, A. A. Ivanov, A. B. Fedotov, A. M. Zheltikov, M.-R. Tsai, M.-C. Chan, C.-H. Yu, and C.-K. Sun, Opt. Express **18**, 24085 (2010).
12. V. Shcheslavskiy, V. V. Yakovlev, and A. Ivanov, Opt. Lett. **26**, 1999 (2001).
13. A. A. Ivanov, B. I. Minkov, G. Jonusauskas, J. Oberlé, and C. Rullière, Opt. Commun. **116**, 131 (1995).
14. F. Krausz, M. E. Fermann, T. Brabec, P. F. Curley, M. Hofer, M. H. Ober, C. Spielmann, E. Wintner, and A. J. Schmidt, IEEE J. Quantum Electron. **28**, 2097 (1992).
15. F. O. Ilday, F. W. Wise, and F. X. Kaertner, Opt. Express **12**, 2731 (2004).
16. Z. Zhang, K. Torizuka, T. Itatani, K. Kobayashi, T. Sugaya, and T. Nakagawa, IEEE J. Quantum Electron. **33**, 1975 (1997).
17. R. L. Fork, C. H. Brito Cruz, P. C. Becker, and C. V. Shank, Opt. Lett. **12**, 483 (1987).
18. F. X. Kärtner, J. A. der Au, and U. Keller, IEEE J. Selected Topics Quantum Electron. **4**, 159 (1998).
19. Y. Chen, F. X. Kärtner, U. Morgner, S. H. Cho, H. A. Haus, E. P. Ippen, and J. G. Fujimoto, J. Opt. Soc. Am. B **16**, 1999 (1999).
20. S. M. J. Kelly, Electron. Lett. **28**, 806 (1992).
21. A. B. Fedotov, A. A. Voronin, I. V. Fedotov, A. A. Ivanov, and A. M. Zheltikov, Opt. Lett. **34**, 851 (2009).
22. V. V. Lozhkarev, G. I. Freidman, V. N. Ginzburg, E. V. Katin, E. A. Khazanov, A. V. Kirsanov, G. A. Luchinin, A. N. Mal'shakov, M. A. Martyanov, O. V. Palashov, A. K. Poteomkin, A. M. Sergeev, A. A. Shaykin, I. V. Yakovlev, S. G. Garanin, S. A. Sukharev, N. N. Rukavishnikov, A. V. Charukhchev, R. R. Gerke, and V. E. Yashin, Opt. Express **14**, 446 (2006).